Nickel-vanadium layered double hydroxide nanosheets as the saturable absorber for passively Q-switched 2 μm solid-state laser

JIANYI XU,[1] ENLIN CAI,[1] SHUAIYI ZHANG,[1,*] XIAOYAN FAN,[1] MINGJIAN WANG,[2] FEI LOU,[1] MAORONG WANG,[1] XIA WANG,[1] AND LIN XU[3]

[1]*Shandong Advanced Optoelectronic Materials and Technologies Engineering Laboratory, School of Mathematics and Physics, Qingdao University of Science & Technology, Qingdao 266061, China*
[2]*Shanghai Key Laboratory of All Solid-State Laser and Applied Techniques, Research Center of Space Laser Information Technology, Shanghai Institute of Optics and Fine Mechanics, Chinese Academy of Sciences, Shanghai, 201800, China*
[3]*Optoelectronics Research Centre, University of Southampton, Southampton, SO17 1BJ, UK*
**Corresponding author: shuaiyi163@163.com*

Abstract: The Nickel-vanadium (NiV)-layered double hydroxide (LDH) was fabricated into a novel saturable absorber (SA) by the liquid phase exfoliation method and was utilized as the laser modulator for the first time. We investigated a passive Q-switched (PQS) Tm:YAG ceramic laser at 2 μm with the NiV-LDH SA. Under an absorbed pump power of 7.2 W, the shortest pulse width of 398 ns was obtained with an average output power of 263 mW and a pulse repetition frequency (PRF) of 101.8 kHz, corresponding to a single pulse energy to be 2.30 μJ. The results indicate that the NiV-LDH SA has great research potential in the field of laser modulation.

1. Introduction

Diode-pumped nanosecond pulsed laser sources at 2 μm have remained a research hotspot in various application fields, such as laser ranging, remote sensing, coherent communications, and surgery [1-3]. The PQS lasers have their own unique advantages in generating nanosecond pulse lasers, due to their simplicity and low cost without the need for high-voltage and RF drivers. As the key element of the PQS laser, the SA plays an important role to produce lasers with narrow pulse width. There are several kinds of SAs for 2 μm lasers so far, such as chromium-doped crystals, commercial SESAMs, and various kinds of two-dimensional (2D) materials ranging from graphene to topological insulators (TIs), black phosphorus (BP) and layered transition-metal dichalcogenides (TMDs), which have been investigated to be promising SAs with many remarkable results [4-15]. However, almost all SAs also have their own disadvantages. For example, the Cr^{2+}-doped crystals (ZnS and ZnSe) have limited operation waveband and relatively high cost. The SESAMs as pulse laser modulators are limited owing to their complicated preparation process and narrow tunable bandwidth, which motivated researchers to explore more novel SAs.

The LDH is an important branch of 2D materials, which is attractive for applications of the supercapacitors and batteries [16, 17]. LDHs possess good quality of tunable composition, unique layered structure, and environmental friendliness. The basic structure of LDHs can be fabricated by replacing a fraction of divalent cations in the brucite lattice with trivalent cations, in order that the positive charge is obtained in the layer, and the positive charge is balanced by intercalation of anions (usually water) between layers. As an outstanding represent of LDHs, several Ni-based LDHs have been reported as electrode materials and catalysts, and almost all the attention recently has been laid on their excellent electrochemical characteristics and method of synthesis and preparation [18-19]. Unfortunately, their optical properties and laser modulation performance as the SAs have not been explored up to the present.

In the other hand, thulium (Tm^{3+}) -doped laser ceramics with various host materials have been demonstrated to be potential laser mediums to generate high power, high efficiency 2 μm laser [20-24]. Among these materials, Tm:YAG ceramic has shown the most significant result for ideal laser application. Up to 65% slope efficiency and power scaling of 52 W have been successively realized respectively [25, 26]. However, there were fewer reports took insight in the PQS laser performance of Tm:YAG ceramic. Only the BP-SA and the Bi_2Te_3 have been employed to test the PQS Tm:YAG ceramic laser operation, and the pulse width of 3.12 μs and 355 ns at 2 μm wavelength was obtained respectively [27, 28].

In this work, we fabricated high-quality NiV-LDH nanosheets and prepared SA by drop-coating NiV-LDH over quartz substrate. The optical properties and laser modulator characteristics of NiV-LDH SA were explored for the first time. A stable 2 μm PQS laser operation with Tm:YAG ceramic was realized. The shortest pulses with 398 ns duration and average output power of 263 mW at repetition rate of 101.8 kHz were obtained, which is the NiV-LDH SA PQS laser reported firstly. The corresponding single pulse energy was calculated to be 2.30 μJ.

2. Fabrication and characterization of the NiV-LDH SA

The NiV-LDH powder was prepared by one-step hydrothermal method [29], and the NiV-LDH SA was fabricated with it by the liquid-phase exfoliation method [30, 31]. At first, nickel chloride and vanadium chloride were mixed with urea in deionized water and stirred for one hour according to a certain molar ratio, and then the solution was transferred to a stainless steel reactor for water bath heating of 12 hours and cooling to room temperature. Next, the NiV-LDH powder sample was obtained with drying under vacuum after subjecting to ultrasonic cleaning and centrifugal separation. Then, the nanoscale bulk NiV-LDH powder sample was prepared with absolute ethanol in 10 ml centrifuge tube and seal. After the centrifuge tube was put into the ultrasonic machine (KQ-400KDE) for 6 hours to disperse and strip large samples into nanosheet structures, and centrifuging at 8000 rpm in 15 minutes to stratify the solution, 20 μL of the supernatant solution was dropwise applied onto the quartz substrate. Finally, after keeping the quartz substrate air-drying at room temperature of 23 °C for 3 hours, the NiV-LDH SA was fabricated successfully.

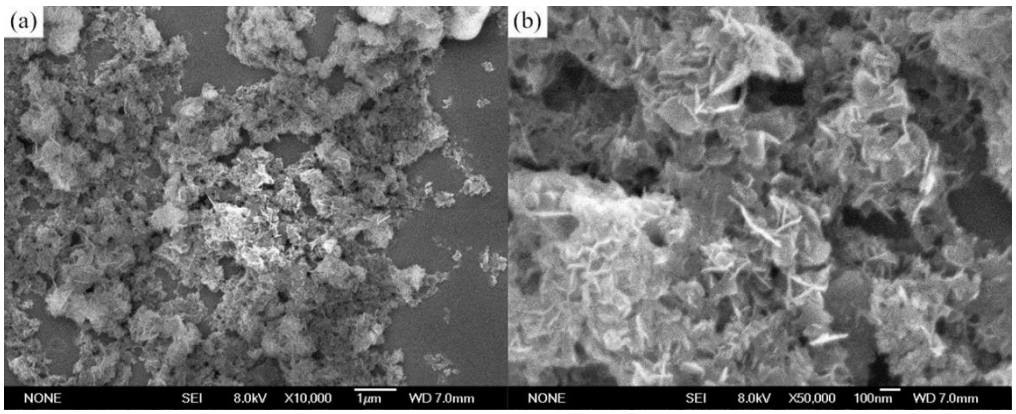

Fig. 1. SEM image of NiV-LDH SA. (a) 1 μm. (b) 100 nm.

The surface morphology of NiV-LDH SA is shown in Fig. 1, which is characterized by a scanning electron microscope (SEM, JSM-6700F, Japan). The laminated structure of the multi-layer nanosheets were clearly visible. The large piece of NiV-LDH was disassembled into small pieces and scattered, which can be seen in Fig. 1(a), and the stacked sheet structure is shown in Fig. 1(b).

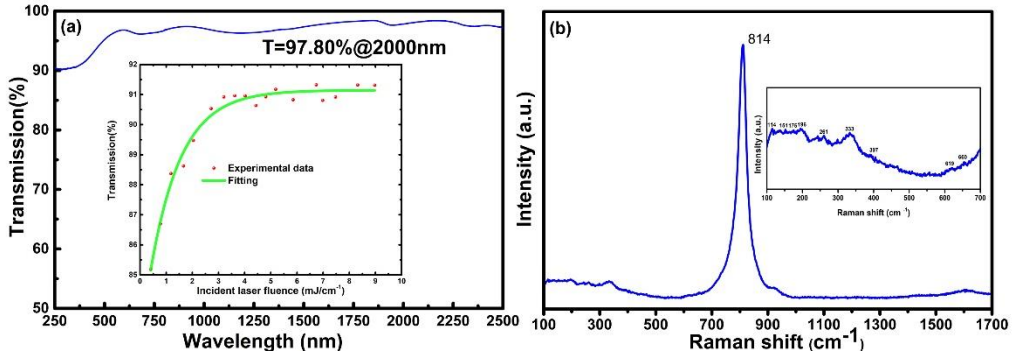

Fig. 2. (a) Linear transmission of NiV-LDH. (a Inset): nonlinear transmission of NiV-LDH SA. (b) Raman spectra of NiV-LDH SA from 100 cm-1 to 1700 cm-1. (b inset) Raman spectra of NiV-LDH SA from 100 cm-1 to 700 cm-1.

The linear transmission of NiV-LDH was measured by UV/VIS/NIR spectrophotometer (CARY500, Varian, American) in the range of 250-2500 nm, as shown in Fig. 2(a), and the transmission was measured to be 97.80% at 2000 nm. The power-dependent nonlinear transmission curve of the NiV-LDH SA was measured by an AOM (QSG27-2000-3QE, CETC) Q-switched Tm:YAP pulsed laser with the pulse width of 400 ns at the PRF of 1 kHz, which was used as laser source at 2 μm. As shown in the Fig. 2(a Inset), the curves result is fitted theoretically by equation (1) [28, 32]:

$$T(\Phi) = 1 - \Delta T \cdot e^{\left(-\frac{\Phi}{\Phi_{sat}}\right)} - T_{ns} \tag{1}$$

Where ΔT, Φ, Φ_{sat} and T_{ns} are the modulation depth, incident laser fluence, saturated incident laser fluence and the non-saturable absorption, respectively. By fitting experimental data, the small-signal transmission is 85.19% with a modulation depth of 8.48%, and the non-saturable absorption of the NiV-LDH SA is calculated to be 8.85%. In addition, the Raman spectra were performed in Fig. 2(b) by Raman spectroscopy (inVia™ InSpect confocal Raman microscope, Renishaw, Britain) under the excitation wavelength of 532 nm. The Raman responses of V-O vibrations bring a strong peak at 814 cm^{-1}, which is consistent with the former report [29]. To verify the stability of NiV-LDH SA, we adopted a pulse laser with the pulse width of 100 ns and the PRF of 1 kHz, to estimate its damage threshold and the damage threshold is calculated to be more than 20 MW/cm^2.

3. Experiment setup and results

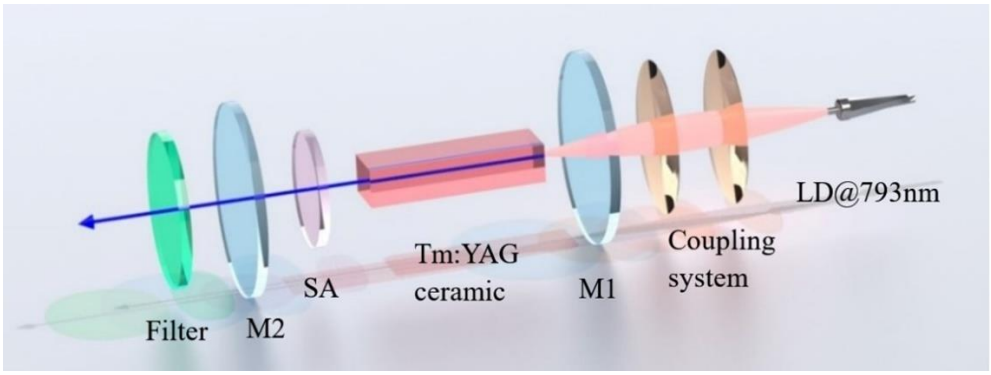

Fig. 3. The experimental setup for the NiV-LDH SA Q-switched Tm: YAG ceramic laser.

A schematic diagram of the experimental setup is depicted in Fig. 3. Through the 1:1 coupling collimation system, the pump light with central wavelength of 793 nm was focused into the Tm:YAG ceramic with dimensions of 3 mm×3 mm×6 mm with Tm^{3+}-doping concentration of 6 at.%. Both sides of the Tm:YAG ceramic were anti-reflection (AR) coated at 780 ± 15 nm and 2000 ± 50 nm. To reduce the thermal effect of the gain medium, it was wrapped in indium foil and placed in a copper sink to water-cool, whose system was kept at 13 °C. Both the input mirror M1 and the output coupler (OC) mirror M2, employed in resonant cavity with the length of 2.7 cm, were plane mirrors. The input mirror M1 was coated with a high reflection from 1820 nm to 2150 nm (R> 99.9%) and an AR at 790 nm. Three flat mirrors with different transmissions of 1%, 3% and 5% at 2 μm were utilized as OCs. After the mirror M2, there was a filter to block the pump light and a power meter (CNI, TS35) was employed to measure the average output power.

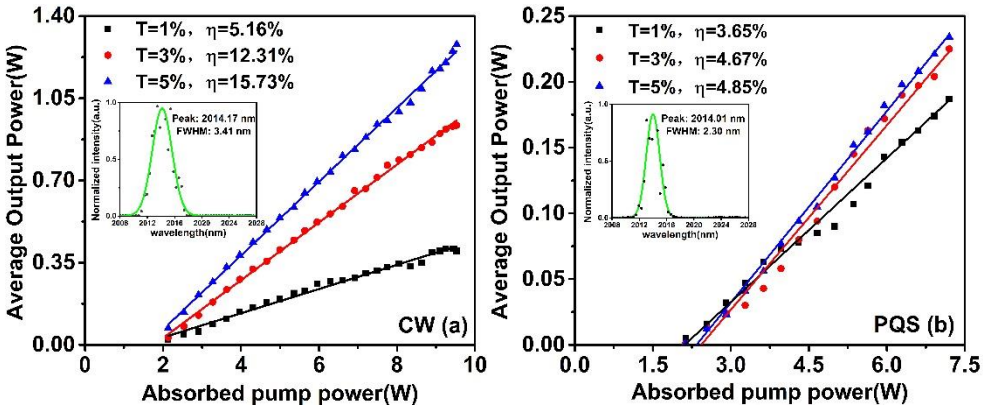

Fig. 4. The average output power versus absorbed pump power with different transmissions and the output spectra (Inset) of the lasers. (a) CW laser. (b) PQS laser.

The average output power versus absorbed pump power of the continuous-wave (CW) laser and PQS laser was measured respectively, with different OC transmissions of 1%, 3%, and 5%. Through the linear fitting, the slope efficiency and threshold power of the CW laser and PQS laser were also calculated and described in Fig. 4. The average output power increases with the absorbed pump power. At the transmittance of OC (T_{OC}) of 5%, the CW output power achieved a maximum output power of 956 mW with a maximum slope efficiency of 15.73%, while the PQS output power gained a maximum output power of 263 mW with a maximum slope efficiency of 4.85%. In terms of threshold power, when the T_{OC} is 5%, PQS laser required a higher threshold power of 2.34 W than CW laser of 1.58 W.

The output spectra of CW laser and PQS laser were measured by spectrometer (APE-waveScan Germany), and the center of spectrum of PQS laser is 2014.01 nm with a narrower FWHM of 2.30 nm, which can be seen in Fig. 4 (b Inset), while the FWHM of the CW laser shown in Fig. 4 (a Inset) under the same condition is 3.41 nm. In addition, the transverse beam quality of the maximum laser output was measured by the 90/10 scanning knife-edge method, and the calculated M^2 factors were 1.65 and 1.53 in tangential and sagittal direction.

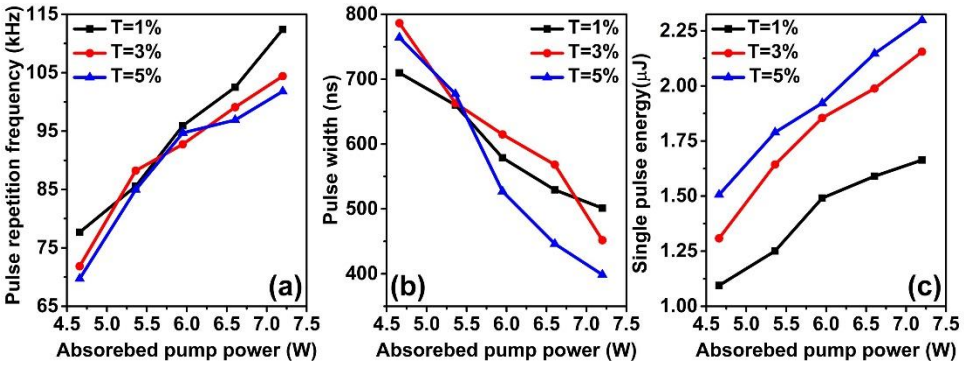

Fig. 5. Performance of the PQS laser. (a) PRF. (b) Pulse width. (c) Single pulse energy.

Using a digital oscilloscope (Tektronix, DPO 4102B-L 1GHz bandwidth 5G samples/s), the PQS laser pulse trains were recorded with an InGaAs PIN detector (EOT, ET-5000). According to the obtained pulse image data and the recorded average output power data, the PRF, the pulse width, and the single pulse energy were calculated, and their variation trends were displayed in Fig. 5(a), (b) and (c).

As seen from Fig. 5(a) and (b), with the absorbed power increasing, the PRF continues to increase, while the pulse width gradually decreases. That is mainly because both the intracavity population inversion densities and the initial population inversion densities at the beginning of the PQS laser will increase by adding the pump power, which usually results in higher PRF and shorter pulses [33]. In addition, From Fig. 5(c), the single pulse energy also risen with the absorbed power increasing. In our experiment, the shortest pulse width of 398 ns was obtained with the PRF of 101.8 kHz at T_{OC}= 5%, corresponding to single pulse energy of 2.30 μJ.

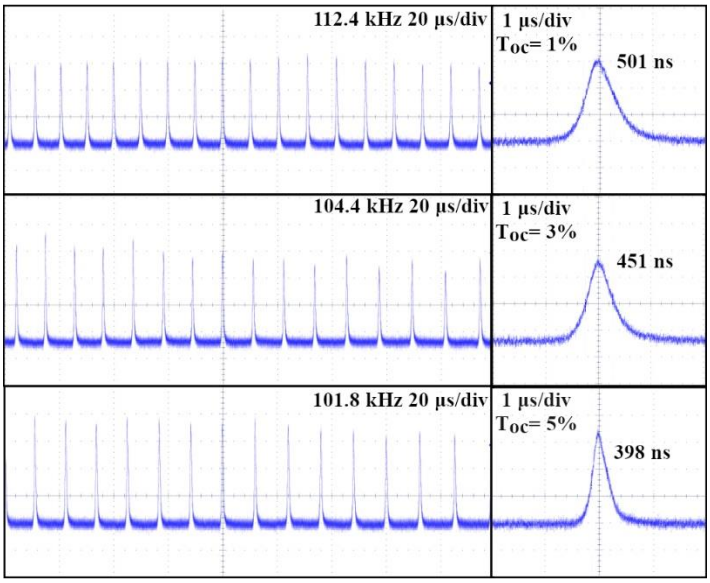

Fig. 6. The temporal pulse trains and the single pulse profiles with different OCs under the absorbed pump power of 7.2 W.

Table 1. Comparisons of the 2 μm PQS laser performance with difference 2D SA materials.

SA Materials	Gain Medium	Pulse Width	PRF	References
WS_2	Tm:LuAG	660 ns	63 kHz	[6]
$MoSe_2$	Tm:LuAG	520 ns	158 kHz	[34]
Bi_2Te_3	Tm:LuAG	233 ns	145 kHz	[35]
Graphene oxide	Tm,Y:CaF_2	1.316 μs	20.22 kHz	[8]
Graphene	Tm:KLuW	190 ns	260 kHz	[36]
MoS_2	Tm,Ho:YAP	435 ns	55 kHz	[37]
g-C_3N_4	Tm:YAP	431 ns	48 kHz	[32]
$ReSe_2$	Tm:YAP	925 ns	89 kHz	[38]
Black phosphorus	Tm:YAP	181 ns	81 kHz	[39]
$MoTe_2$	Tm:YAP	380 ns	144 kHz	[40]
WTe_2	Tm:YAP	368 ns	78 kHz	[41]
$SnSe_2$	Tm:YAP	400 ns	109 kHz	[42]
Gold nanorods	Tm:YAG	796 ns	77 kHz	[43]
Black phosphorus	Tm:YAG ceramic	3.12 μs	11.6 kHz	[27]
Bi_2Se_3	Tm:YAG ceramic	355 ns	117 kHz	[28]
NiV-LDH	Tm:YAG ceramic	398 ns	101 kHz	This work

To demonstrate the pulse stability, the traces and the single pulse profiles in long range oscilloscope with OCs of different transmissions were displayed in Fig. 6, under the absorbed pump power of 7.2 W. The peak-to-peak fluctuation of the pulse sequence in Fig. 6 was less than 10%. To compare the effects of various 2D SA materials on laser modulation, Table 1 lists their performance under Tm^{3+}-doped lasers.

4. Conclusion

In conclusion, we have prepared SAs with NiV-LDH for the first time and investigated their linear and nonlinear optical characteristics. Using NiV-LDH SA, a PQS Tm:YAG ceramic laser at 2 μm was demonstrated, with the shortest pulse width of 398 ns, and the PRF of 101.8 kHz under the pump absorbed power of 7.2 W, corresponding to the single pulse energy of 2.30 μJ. The results indicate that the new 2D SA material based on NiV-LDH, has a very promising value for laser modulation at 2 μm.

Acknowledgments

This work is supported by Natural Science Foundation of Shandong Province (ZR2019MF061) and National Natural Science Foundation of China (No. 62005139 and No. 61905127).

Disclosures

The authors declare no conflicts of interest.

References

1. H. Chen, E. Wu, and H. Zeng, "Comparison between a-cut and off-axially cut Nd:YVO_4 lasers passively Q-switched with a Cr^{4+}:YAG crystal," Opt. Commun. **230**(1-3)**,** 175-180 (2004).
2. Y. P. Chen, Y. P. Lan, and H. L. Chang, "Analytical model for design criteria of passively Q-switched lasers," IEEE J. Quantum Electron. **37**(3)**,** 462-468 (2001).
3. X. Feng, J. Liu, W. Yang, X. Yu, S. Jiang, T. Ning, and J. Liu, "Broadband indium tin oxide nanowire arrays as saturable absorbers for solid-state lasers," Opt. Express **28**(2)**,** 1554-1560 (2020).
4. D. Sebbag, A. Korenfeld, U. Ben-Ami, D. Elooz, E. Shalom, and S. Noach, "Diode end-pumped passively Q-switched Tm:YAP laser with 1.85-mJ pulse energy," Opt. Lett. **40**(7), 1250-1253 (2015).
5. B. Yao, Y. Tian, G. Li, and Y. Wang, "InGaAs/GaAs saturable absorber for diode-pumped passively Q-switched dual-wavelength Tm:YAP lasers," Opt. Express **18**(13), 13574–13579 (2010).
6. C. Luan, K. Yang, J. Zhao, S. Zhao, L. Song, T. Li, H. Chu, J. Qiao, C. Wang, Z. Li, S. Jiang, B. Man, and L. Zheng, "WS_2 as a saturable absorber for Q-switched 2 micron lasers," Opt. Lett. **41**(16)**,** 3783-3786 (2016).
7. Y. Yao, N. Cui, Q. Wang, L. Dong, and J. He, "Highly efficient continuous-wave and $ReSe_2$ Q-switched ~3 μm dual-wavelength Er:YAP crystal lasers," Opt. Lett. **44**(11)**,** 2839-2942 (2019).
8. C. Zhang, J. Liu, X. Fan, Q. Peng, X. Guo, D. Jiang, X. Qian, and L. Su, "Compact passive Q-switching of a diode-pumped Tm,Y:CaF_2 laser near 2 μm," Opt. Laser Technol. **103,** 89-92 (2018).
9. H. Liu, Z. Sun, X. Wang, Y. Wang, and G. Cheng, "Several nanosecond Nd:YVO_4 lasers Q-switched by two dimensional materials: tungsten disulfide, molybdenum disulfide, and black phosphorous," Opt. Express **25**(6)**,** 6244-6252 (2017).
10. S. Wang, H. Yu, H. Zhang, A. Wang, M. Zhao, Y. Chen, L. Mei, and J. Wang, "Broadband few-layer MoS_2 saturable absorbers," Adv. Mater. **26**(21)**,** 3538-3544 (2014).
11. N. Cui, F. Zhang, Y. Zhao, Y. Yao, Q. Wang, L. Dong, H. Zhang, S. Liu, J. Xu, and H. Zhang, "The visible nonlinear optical properties and passively Q-switched laser application of a layered $PtSe_2$ material," Nanoscale **12**(2)**,** 1061-1066 (2020).
12. P. Ge, J. Liu, S. Jiang, Y. Xu, and B. Man, "Compact Q-switched 2 μm Tm:$GdVO_4$ laser with MoS_2 absorber," Photonics Res. **3**(5)**,** 256-259 (2015).
13. Q. Yang, F. Zhang, N. Zhang, and H. Zhang, "Few-layer MXene $Ti_3C_2T_x$ (T= F, O, or OH) saturable absorber for visible bulk laser," Opt. Mater. Express **9**(4)**,** 1795-1802 (2019).
14. X. Wu, M. Yun, M. Wang, C. Liu, K. Li, X. Qin, W. Kong, and L. Dong, "Self-imaging in multi-walled carbon nanotube arrays at visible wavelengths," Carbon **108,** 47-51 (2016).
15. J. Liu, Y. Wang, Z. Qu, and X. Fan, "2 μm passive Q-switched mode-locked Tm^{3+}:YAP laser with single-walled carbon nanotube absorber," Opt. Laser Technol. **44**(4)**,** 960-962 (2012).
16. H. W. Park, J. S. Chae, S. Park, K. Kim, and K. C. Roh, "Nickel-based layered double hydroxide from guest vanadium oxide anions," Met. Mater. Int. **19**(4)**,** 887-894 (2013).
17. S. Wang, S. Lai, P. Li, T. Gao, K. Sun, X. Ding, T. Xie, C. Wu, X. Li, Y. Kuang, W. Liu, W. Yang, and X. Sun, "Hierarchical cobalt oxide@Nickel-vanadium layer double hydroxide core/shell nanowire arrays with enhanced areal specific capacity for nickel-zinc batteries," J. Power Sources **436,** 226867 (2019).
18. A. Tyagi, M. Chandra Joshi, K. Agarwal, B. Balasubramaniam, and R. K. Gupta, "Three-dimensional nickel vanadium layered double hydroxide nanostructures grown on carbon cloth for high-performance flexible supercapacitor applications," Nanoscale Adv. **1**(6)**,** 2400-2407 (2019).
19. T. Wang, S. Zhang, X. Yan, M. Lyu, L. Wang, J. Bell, and H. Wang, "2-methylimidazole-derived Ni-Co layered double hydroxide nanosheets as high rate capability and high energy density storage material in hybrid supercapacitors," ACS Appl. Mater. Interfaces **9**(18)**,** 15510-15524 (2017).
20. G. A. Caravaggio, C. Detellier, and Z. Wronski, "Synthesis, stability and electrochemical properties of NiAl and NiV layered double hydroxides," J. Mater. Chem. **11**(3)**,** 912-921 (2001).
21. S. Zhang, M. Wang, L. Xu, Y. Wang, Y. Tang, X. Cheng, W. Chen, J. Xu, B. Jiang, and Y. Pan, "Efficient Q-switched Tm:YAG ceramic slab laser," Opt. Express **19**(2)**,** 727-732 (2011).
22. Z. Hao, L. Zhang, Y. Wang, H. Wu, G. Pan, H. Wu, X. Zhang, D. Zhao, and J. Zhang, "11 W continuous-wave laser operation at 2.09 μm in Tm:$Lu_{1.6}Sc_{0.4}O_3$ mixed sesquioxide ceramics pumped by a 796 nm laser diode," Opt. Mater. Express **8**(11)**,** 3615-3621 (2018).
23. H. Zhu, Y. Zhang, J. Zhang, Y. Zhang, Y. Duan, X. Ruan, J. Zhang, and D. Tang, "1.96-μm Tm:YAG ceramic laser," IEEE Photon. J. **9**(6)**,** 1-7 (2017).
24. Z. Zhou, X. Guan, X. Huang, B. Xu, H. Xu, Z. Cai, X. Xu, P. Liu, D. Li, J. Zhang, and J. Xu, "Tm^{3+}-doped $LuYO_3$ mixed sesquioxide ceramic laser: effective 2.05 μm source operating in continuous-wave and passive Q-switching regimes," Opt. Lett. **42**(19)**,** 3781-3784 (2017).
25. W. L. Gao, J. Ma, G. Q. Xie, J. Zhang, D. W. Luo, H. Yang, D. Y. Tang, J. Ma, P. Yuan, and L. J. Qian, "Highly efficient 2 μm Tm:YAG ceramic laser," Opt. Lett. **37**(6)**,** 1076-1078 (2012).
26. X. Liu, H. Huang, D. Shen, X. Fan, W. Yao, H. Zhu, J. Zhang, and D. Tang, "High-power LD end-pumped Tm:YAG ceramic slab laser," Appl. Phys. B-Lasers Opt. **118**(4)**,** 533-538 (2015).
27. G. Xie, Y. Xie, L. Kong, Z. Qin, and J. Zhang, "Black phosphorus-based saturable absorber for Q-switched Tm:YAG ceramic laser," Opt. Eng. **55**(8)**,** 81307 (2016).
28. J. Shang, T. Feng, S. Zhao, T. Li, Z. Pan, and J. Zhao, "Saturable absorption characteristics of Bi_2Se_3 in a 2 μm Q-switching bulk laser," Opt. Express **28**(4)**,** 5639-5647 (2020).

29. D. Wang, Q. Li, C. Han, Q. Lu, Z. Xing, and X. Yang, "Atomic and electronic modulation of self-supported nickel-vanadium layered double hydroxide to accelerate water splitting kinetics," Nat. Commun. **10**(1)**,** 1-12 (2019).
30. C. Huo, Z. Yan, X. Song, and H. Zeng, "2D materials via liquid exfoliation: a review on fabrication and applications," Sci. Bull. **60**(23)**,** 1994-2008 (2015).
31. J. N. Coleman, M. Lotya, A. O'Neill, S. D. Bergin, P. J. King, U. Khan, K. Young, A. Gaucher, S. De, R. J. Smith, I. V. Shvets, S. K. Arora, G. Stanton, H. Kim, K. Lee, G. T. Kim, G. S. Duesberg, T. Hallam, J. J. Boland, J. J. Wang, J. F. Donegan, J. C. Grunlan, G. Moriarty, A. Shmeliov, R. J. Nicholls, J. M. Perkins, E. M. Grieveson, K. Theuwissen, D. W. McComb, P. D. Nellist, and V. Nicolosi, "Two-dimensional nanosheets produced by liquid exfoliation of layered materials," Science **331**(6017)**,** 568-571 (2011).
32. Z. Niu, G. Li, K. Yang, T. Li, J. Zhao, S. Zhao, D. Li, W. Qiao, H. Chu, T. Feng, K. Gao, Q. Qian, and H. Ma, "Doubly Q-switched Tm:YAP laser with g-C_3N_4 saturable absorber and AOM," Opt. Mater. **96,** 109306 (2019).
33. S. Zhang, X. Liu, L. Guo, M. Fan, F. Lou, P. Gao, G. Guo, J. Yang, J. Liu, T. Li, K. Yang, S. Zhao, J. Liu, J. Xu, and Y. Hang, "Passively Q-switched Ho,Pr:LLF bulk slab laser at 2.95 μm based on MoS_2 saturable absorber," IEEE Photon. Technol. Lett. **29**(24)**,** 2258-2261 (2017).
34. X. Liu, K. Yang, S. Zhao, M. Li, W. Qiao, T. Li, S. Zhang, L. Zheng, L. Su, J. Xu, and J. Bian, "High repetition rate all-solid-state pulsed 2 μm laser based on selenide molybdenum saturable absorber," IEEE J. Sel. Top. Quantum Electron. **24**(5)**,** 1-6 (2017).
35. J. Qiao, S. Zhao, K. Yang, W. Song, W. Qiao, C. Wu, J. Zhao, G. Li, D. Li, T. Li, H. Liu, and C. Lee, "High-quality 2-μm Q-switched pulsed solid-state lasers using spin-coating-coreduction approach synthesized Bi_2Te_3 topological insulators," Photonics Res. **6**(4)**,** 314-320 (2018).
36. A. S. Yasukevich, P. Loiko, N. V. Gusakova, J. M. Serres, X. Mateos, K. V. Yumashev, N. V. Kuleshov, V. Petrov, U. Griebner, M. Aguiló, and F. Díaz, "Modelling of graphene Q-switched Tm lasers," Opt. Commun. **389,** 15-22 (2017).
37. C. Luan, X. Zhang, K. Yang, J. Zhao, S. Zhao, T. Li, W. Qiao, H. Chu, J. Qiao, J. Wang, L. Zheng, X. Xu, and J. Xu, "High peak power passively Q-switched 2 μm laser with MoS_2 saturable absorber," IEEE J. Sel. Top. Quantum Electron. **23**(1)**,** 66-70 (2016).
38. Y. Yao, X. Li, R. Song, N. Cui, S. Liu, H. Zhang, D. Li, Q. Wang, Y. Xu, and J. He, "The energy band structure analysis and 2 μm Q-switched laser application of layered rhenium diselenide," RSC Adv. **9**(25)**,** 14417-14421 (2019).
39. H. Zhang, J. He, Z. Wang, J. Hou, B. Zhang, R. Zhao, K. Han, K. Yang, H. Nie, and X. Sun, "Dual-wavelength, passively Q-switched Tm:YAP laser with black phosphorus saturable absorber," Opt. Mater. Express **6**(7)**,** 2328-2335 (2016).
40. B. Yan, B. Zhang, H. Nie, H. Wang, G. Li, X. Sun, R. Wang, N. Lin, and J. He, "High-power passively Q-switched 2.0 μm all-solid-state laser based on a $MoTe_2$ saturable absorber," Opt. Express **26**(14)**,** 18505-18512 (2018).
41. L. Chen, X. Li, H. Zhang, and W. Xia, "Passively Q-switched 1.989 μm all-solid-state laser based on a WTe_2 saturable absorber," Appl. Opt. **57**(35)**,** 10239-10242 (2018).
42. X. Liu, Q. Yang, C. Zuo, Y. Cao, X. Lun, P. Wang, and X. Wang, "2-μm passive Q-switched Tm:YAP laser with $SnSe_2$ absorber," Opt. Eng. **57**(12)**,** 126105 (2018).
43. H. Huang, M. Li, P. Liu, L. Jin, H. Wang, and D. Shen, "Gold nanorods as the saturable absorber for a diode-pumped nanosecond Q-switched 2 μm solid-state laser," Opt. Lett. **41**(12)**,** 2700-2703 (2016).